Journal of Building Engineering 113 (2025) 114144

Contents lists available at ScienceDirect

Journal of Building Engineering

journal homepage: www.elsevier.com/locate/jobe

The influence of aggregate content and aggregate grading on the air bubble rise in fresh concrete

Bastian Strybny [a,*], Max Coenen [a], Valérie Vidal [b], Tobias Schack [a], Marcus Zuber [c], Michael Haist [a]

[a] Institute of Building Materials Science, Leibniz University Hannover, Germany
[b] Laboratoire de Physique, ENS de Lyon, CNRS, France
[c] Institute for Photon Science and Synchrotron Radiation, Karlsruhe Institute of Technology, Germany

ARTICLE INFO

Keywords:
Concrete
De-airing
Air bubble
Aggregate grading
Particle migration
X-ray

ABSTRACT

The durability and mechanical properties of hardened concrete are significantly affected by its porosity. Air voids can be trapped in fresh concrete during placement, particularly when insufficient workability is combined with inadequate processing. The mechanisms by which air bubbles rise in fresh concrete and interact with surrounding aggregates remain largely unknown.

This study investigates how the rheological and granulometrical characteristics of fresh concrete affect de-airing behavior. Due to the opacity of concrete, X-ray techniques coupled to digital image analysis were used to study the bubble dynamics and the bubble-aggregate interactions. Concrete is idealised as a mix of glass beads as model aggregates ($d_a \leq 8$ mm) suspended in a cement-water suspension, termed cement paste. The investigation focused on the relationship between the cement paste rheology, the aggregate properties and the speed, shape and trajectory of rising air bubbles. Further the effect of shear history and shear-induced particle migration on bubble rise was also investigated. The results show that the addition of aggregates to pure cement paste significantly alters the de-airing behavior and affects the bubble dynamics. As the bubble volume decreases, the bubble speed decreases. Increasing the aggregate content from 0 vol% to either 30 vol% or 60 vol% also results in a decrease in bubble speed. Small bubbles show minimal variation in rise trajectories across different aggregate volumes and gradings. In contrast, larger bubbles exhibit consistent paths with 30 vol% aggregates, but demonstrate dispersed trajectories at 60 vol%. Shear-induced particle migration depends on the bubble-to-aggregate size ratio. Finally, a dimensionless parameter is introduced that can be used to determine phase separation as a function of the ratio of bubble buoyancy to aggregate inertia. This research improves the understanding of concrete de-airing and is also applicable to other coarse granular suspensions in various industries.

1. Introduction

Fresh concrete undergoes several stages in the production cycle. Besides mixing, transport and placement and in particular the compaction process is crucial for ensuring durability and mechanical performance. Until now, the necessary intensity of concrete

* Corresponding author.
E-mail address: b.strybny@baustoff.uni-hannover.de (B. Strybny).

https://doi.org/10.1016/j.jobe.2025.114144
Received 2 June 2025; Received in revised form 18 September 2025; Accepted 20 September 2025
Available online 24 September 2025

compaction is solely derived from the fresh concrete consistency in a qualitative manner. However, the concrete composition and more complex rheological characteristics such as thixotropy are not taken into account, despite the fact that e.g. w/c ratio, paste content, or aggregate granulometry mainly control the flow behavior and therefore the de-airing of the fresh concrete [1–3]. In particular, aggregate size, distribution and shape determine the amount of paste required to achieve a given consistency. The paste demand is therefore correlated with the packing density, which is defined as the ratio of the volume of solids to the bulk volume.

The main parameter determining the packing density of the aggregates is the particle size distribution (PSD), i.e. having particles of different sizes in different proportions. The PSD should be chosen so that the voids between the coarse particles are perfectly filled with finer particles and so forth. With regard to concrete, substantial work on the maximum packing density by tuning the PSD was done as early as 1907 e.g. by Fuller and Thompson [4], Andreasen [5] and Funk and Dinger [6]. Whereas these models allow to predict a PSD which yields a high packing density, the true packing density remains unkown and pronounced model idealizations significantly limit the prediction accuracy. Extended models such as those of de Larrad [7] and its extension of Fennis [8] included information on particle shape etc., however, are labourintensive in their calibration. Experimental studies on the compaction of dry aggregates at constant compaction intensity have shown that, for example, round-shaped sand and gravel with smooth surfaces yield higher packing densities than flaky grains. Better packing was also achieved by increasing the compaction intensity. Frictional forces due to the aggregates' angularity must also be considered in the mix design as they can influence the workability and compaction [9]. Both the maximum (intrinsic) packing density as well as the cement paste content in the concrete influence both the fresh as well as the hardened state concrete properties. In the fresh state, packing optimization can be used to enhance workability and segregation stability, whether in conventional vibrated concrete or in the design of high flowable concretes and self-compacting concretes [7,10]. Other benefits of optimised packaging can also be seen in the improved properties of the hardened concrete, as packing optimization goes hand in hand with a reduction in void ratio and paste content and therefore less creep and shrinkage, heat of hydration, cost and, most importantly, CO_2 emission savings [9,11].

Despite its importance, the packing density has mainly been discussed in terms of workability and stability. Its effect on the concrete de-airing mechanisms remains more or less unkown. Macroscopically, an increased packing reduces the paste content and thus the space and ability of air bubbles to rise to the surface. The current literature treats concrete de-airing mainly as a problem of entrapped air bubbles in hardened concrete. However, the actual mechanisms of concrete de-airing and the unsolved dynamic rising process in fresh concrete remains unknown. First investigations on this subject have been presented by the authors by investigating the dynamic mechanisms of bubble rise in cement suspensions, as well as the influence of coarse aggregates in a monodisperse PSD on bubble rise, by means of optical investigations using X-ray analysis [3,12]. However, the influence of polydisperse PSD on bubble rise still remains an open scientific question.

The paper at hand presents a comprehensive study of bubble rise with different bubble volumes in different concrete compositions. It focuses on the influence of aggregates on the dynamics of air bubble rise in fresh concrete. The properties of real aggregates used in concrete production are very complex due to their varying mineral composition, size and size distribution, shape, surface texture and moisture content. These factors can significantly affect the workability and overall performance of the concrete mix. It is therefore common in the literature to use spherical model aggregates for reasons of simplicity, however, these model systems were used for investigating the pumping behavior of concrete and not the de-airing behavior [13–15]. The use of such model aggregates reduces the complexity of varying aggregate properties and allows the focus to be on defined boundary conditions such as the effect of aggregate content and aggregate grading. When transferring the results from this model to real aggregates, it must be taken into account that the shape, surface smoothness and composition may impact the flowability of fresh concrete, due to different packing and with that also the de-airing behavior. The bubble volume was varied in 3 steps and the concretes were made with 2 different aggregate volume fractions (30 vol% and 60 vol%) and 2 different aggregate gradings (coarse and fine PSD). A pure cement paste was also included in this study for reference. In addition to these granulometry effects on the bubble rise parameter (e.g. bubble speed, trajectory or deformations), the effect of shear history and shear-induced particle migration on de-airing was also investigated.

2. Materials and methods

2.1. Raw materials and mix properties

The present research was part of the German Priority Program DFG SPP 2005 program 'Opus Fluidum Futurum – Rheology of reactive, multiscale, multiphase construction materials'. The cement paste was prepared using Ordinary Portland Cement CEM I 42.5 R, supplied by Heidelberg Materials AG (Ennigerloh plant, Germany); details see Ref. [16]. The relevant phyiscal properties i.e. density [17], specific surface area SSA by Blaine and BET method [18,19] and particle size distribution measured by laser diffraction method [20] are given in Table 1. The oxide compositon of the cement was measured by XRF [21] and is shown in Table 2.

In this study, spherical beads of polished soda glass (Hilgenberg GmbH, Malsfeld, Germany) of sizes 2.0 ± 0.2 mm, 4.0 ± 0.3 mm,

Table 1
Physical properties of the investigated cement.

Component	Density [g/cm^3]	Specific surface area		Granulometrical parameters		
		SSA_{Blaine} [cm^2/g]	SSA_{BET} [m^2/g]	d_{10} [µm]	d_{50} [µm]	d_{50} [µm]
CEM I 42.5 R	3.14	3499	1.04	1.92	14.10	41.49

and 8.0 ± 0.4 mm respectively, were used as model aggregates. The density of the 2 mm and 4 mm model aggregates was 1.50 kg/dm^3, the density of the 8 mm aggregates was 1.48 kg/dm^3. The aggregates were used in two different polydisperse distributions, one with a higher content of coarse aggregates and one with a higher content of fine aggregates compared to a reference grading curve A/B8 according to DIN 1045–2 [22] shown in Fig. 1. The coarse grading curve consists of 36 % by volume 2 mm, 25 % by volume 4 mm and 39 % by volume 8 mm aggregates. The fine grading curve is made up of 57 vol% 2 mm, 17 vol% 4 mm and 26 vol% 8 mm aggregates.

Both the fine and coarse distributions were used in aggregate volume fractions of 30 vol% ($\phi_a = 0.30$) and 60 vol% ($\phi_a = 0.60$). The phase content of the cement paste was kept constant at 38 vol% ($\phi_p = 0.38$), corresponding to a water/cement ratio of 0.52. This results in five different mixtures. The mix compositions are given in Table 3.

The mixing procedure of the model-concretes is detailed in Table 4.

After concrete preparation, a Hägerman spread flow test (according to DIN EN 1015–3 [23]) without shocks was carried out to measure the spread flow of the mixture. Further the temperature of the fresh mix was measured. The rheology of the cement paste was measured by a Haake Mars 60 Rheometer (ThermoFisher Scientific, Karlsruhe, Germany) with a building material cell and window-shaped paddle (geometry P-3 acc. To Ref. [24]). Further information on the procedure can be found in Ref. [25]. The surface tension of the fresh cement paste was determined using an Attension Theta Flow optical tensiometer (Biolin Scientific, Goeteborg, Sweden). A full description on the sample characterization procedure employed in this study can be found in Ref. [3].

2.2. Cement paste and concrete properties

The cement paste was measured to have a yield stress of 10.64 Pa, a plastic viscosity of 0.18 Pa s, a surface tension of 33.93 mN/m and a spread flow of 260 mm. By adding 30 vol% of aggregates, the spread flow remains almost constant both when coarse as well as fine aggregates are used. The effects of the aggregates become more visible when the aggregate content reaches 60 vol% as the spread flow is reduced to 210 mm for the coarse and to 207.5 mm for the fine graded aggregates. The temperature of the suspensions was between 20.2 °C and 22.5 °C.

2.3. Experimental de-airing setup

Since cement paste and fresh concrete are opaque granular suspensions, all the de-airing tests were carried out at the X-ray laboratory of the Institute for Photon Science and Synchrotron Radiation (IPS), Karlsruhe Institute of Technology, Germany. Using this setup the dynamics of rising air bubbles in such opaque systems were characterized. Technical information on the development of the de-airing setup can be found in Refs. [3,26].

The de-airing setup consists of a rectangular Plexiglas column measuring 650 x 75 × 75 mm^3 (height x width x depth) with a wall thickness of 5 mm. The column is firmly glued to a stainless steel baseplate which is mounted to a vertically movable stage in the X-ray laboratory. The stage allows the sample to be ideally positioned between the X-ray source and the detector. For bubble injection, a 5 mm diameter tube is inserted at the bottom of the column. The tube is connected to an electronically controlled valve with time control adjustable time steps of 5 ms. The tube is connected to a pressure regulator set to a constant air pressure of 1.00 bar. This setup allows for a flow rate controlled injection of different bubble sizes, but not volume-controlled injection, resulting in very small variations in bubble volume even for the same injection duration, as the air bubble volume forming in the fresh paste or concrete is not only a function of the valve opening duration but also of the paste or concrete rheology (see Fig. 3 (right)).

The X-ray worked with 220 kV and 280 W target power. The frame rate of the image acquisition was set to 30 fps, which allows a frame-based two-dimensional quantification of the bubbles geometry and the position within the sample column as a function of time. To determine these parameters, we developed an evaluation algorithm based on semantic image segmentation. The algorithm automatically separates the bubble from the surrounding fresh concrete based on a threshold value and finally computes all required bubble characteristics framewise. The resolution per pixel was 0.28 mm. This study focused on bubble volume, bubble speed, bubble centroid in the *x* and *y* direction (compare Fig. 2 (right)), trajectory and bubble deformation due to interactions with the aggregates.

3. Experimental results and discussion

3.1. General observations

As described in sec 2.2 the geometrical shape, position and rise speed of the bubbles were derived from digital image analysis of the X-ray data. The employed image evaluation algorithm calculates the bubble volume by assuming rotational symmetry. As the bubble shape changes due to interactions with the aggregates, Fig. 3 (left) shows these changes in bubble volume during the vertical bubble rise for the two most critical mixture compositions with 60 vol% of aggregates. It can be seen that the bubble volume increases at the

Table 2
Oxide composition of the investigated cement [21].

Component	CaO	SiO_2	Al_2O_3	Fe_2O_3	MgO	K_2O	Na_2O	TiO_2	P_2O	Mn_2O_3	SO_3	LOI	Cl^-	Sum
	[wt%]													
CEM I 42.5 R	61.79	21.14	5.53	2.27	1.39	0.77	0.77	0.21	0.14	0.03	2.84	2.48	0.03	98.94

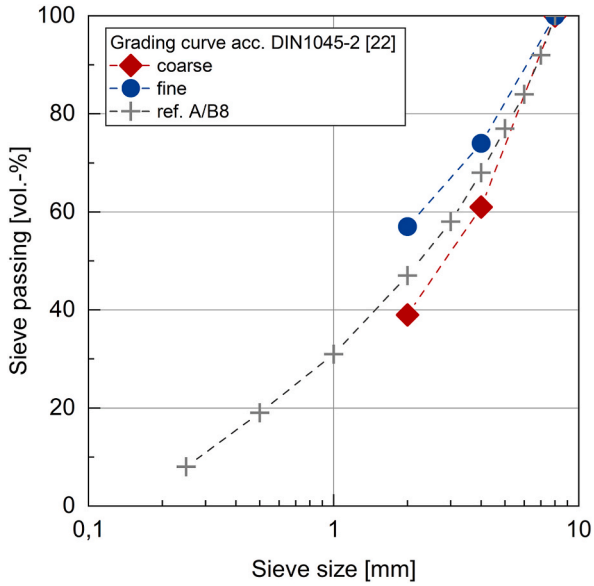

Fig. 1. Cummulative grading curves of the investigated model-aggregates and a reference grading curve A/B8 acc. DIN 1045–2 [22].

Table 3
Mix composition of the investigated concretes; mix volume 3 dm^3.

Mix ID ϕ_p_ ϕ_a_d_a	Cement [g]	Water [g]	Aggregate volume fraction ϕ_a [−]	Aggregates $d_a = 2$ mm [g]	Aggregates $d_a = 4$ mm [g]	Aggregates $d_a = 8$ mm [g]
0.38_0_0	3580	1860	0	0	0	0
0.38_0.3_coarse	2506	1302	0.3	486	338	519
0.38_0.6_coarse	1432	744	0.6	972	675	1039
0.38_0.3_fine	2506	1302	0.3	770	230	346
0.38_0.6_fine	1432	744	0.6	1539	459	693

Table 4
Concrete mixing procedure.

Time [min]	Step description	Duration [sec]
0–0:30	Pouring and mixing of components by hand	30
0:30–1:30	Mixing at lower speed	90
1:30–3:00	Manual return of caking material	90
3:00–4:30	Mixing at higher speed	90
4:30–5:00	Manual return of caking material	30
5:00–6:00	Mixing at higher speed	60
6:00–12:30	Rest	390
12:30–13:00	Re-mixing at lower speed	30
13:00–14:00	Manual addition and mixing of model-aggregates	60

bottom as this describes the injection process and the formation of the bubble. The volume decreases at the top as the bubble leaves the field of view of the X-ray detector. In order to avoid such artefacts a region of interest (ROI) was therefore introduced and used to further calculate all the bubble parameters studied in this paper (see Fig. 3 (left), gray region). Looking more closely at the bubble volume in this ROI, significant changes in volume can be seen, but the volume scatters around the mean value. The bubble deforms in all directions, i.e. if the measured bubble volume decreases in the x and y planes, the bubble will also deform in the z direction. For further evaluation, we therefore use the average bubble volume in the ROI.

Another observation, already described in Refs. [3,12], is that the test set-up only allows for flow rate controlled air injection and not volume controlled injection. Fig. 3 (right) shows the resulting mean bubble volume as a function of air injection duration. The data points are related using linear regression. It can be seen that for the mixtures investigated, the same injection duration results in slight variations of bubble volume, however, the mean bubble volume increases almost linear with increasing air injection duration for all mixtures.

Fig. 4 (a)–(c) show the vertical ascent distance of the bubble centroid as a function of ascent duration for different air injection durations of 70 ms, 110 ms and 150 ms, respectively. The slope of these curves determined by linear regression in the ROI is in the

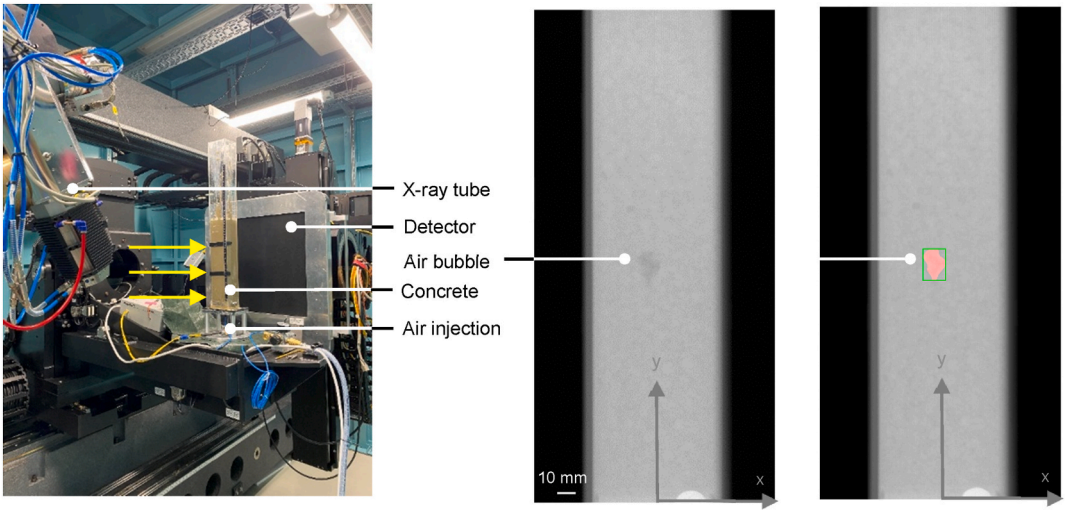

Fig. 2. Test setup in the X-ray lab at IPS KIT (left) and X-ray images of an air bubble before semantic segmentation (middle); with a bounding box after semantic segmentation (right).

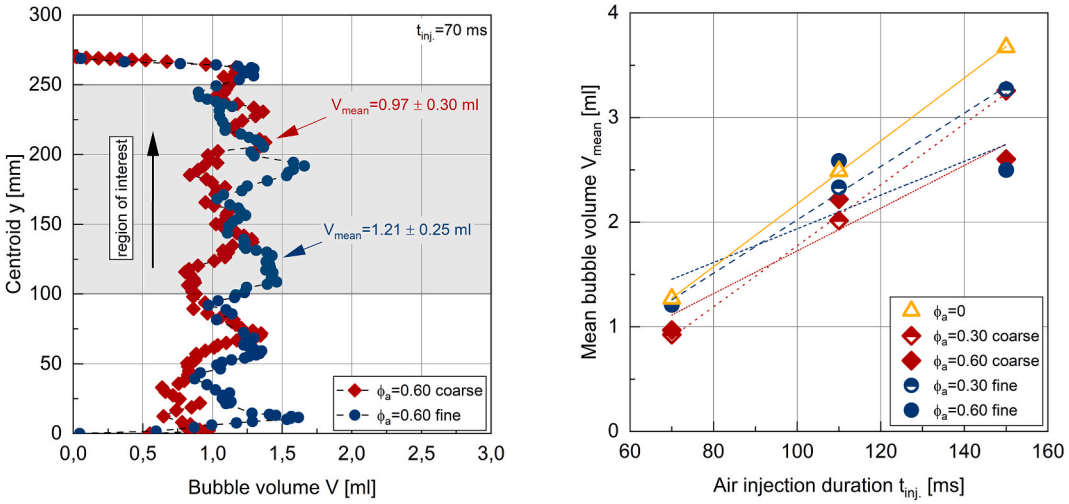

Fig. 3. Changes in bubble volume V during vertical rise calculated from the bubbles 2D contour by assumming rotational symmetry (left) and mean bubble volume V_{mean} as a function of the air injection duration $t_{inj.}$ (right).

following designated as mean bubble speed v_{mean}. For the pure paste, the suspension acts as an effective fluid and the bubble rises with almost constant speed. When aggregates are added at volume fractions of 30 vol% and 60 vol%, the velocity of the bubbles not only decreases but also begins to fluctuate, indicating that the bubble accelerates, stops and re-accelerates as it begins to interact with the aggregates. This effect becomes more dominant with increasing bubble volume V. For further processing, we calculated the bubble velocity v_{mean} as mean values for all bubble volumes V and mixtures studied. The results are shown in Fig. 4 (d). The data shows an almost linear increase in bubble velocity with increasing bubble volume due to buoyancy. The linear relationship can now be used to determine the bubble speed for air bubbles of equivalent volumes V_1, V_2 and V_3. Herefore we have introduced three reference bubble volumes $V_1 = 1$ ml, $V_2 = 2$ ml and $V_3 = 3$ ml and calculated the corresponding bubble speeds by the factor κ. This correction factor makes it possible to compare the effect of flowabiltiy due to mixture composition for bubbles of the same size. From Fig. 4 (d) it can already be deduced that the addition of aggregates to the cement paste reduces the bubble speed depending on the aggregate content and aggregate grading.

3.2. Bubble rise speed

Fig. 5 (a) shows the steady state bubble speed as a function of aggregate volume fraction and bubble volume considering size corrected reference bubbles with volumes V_1 to V_3 (see sec 3.1). A decrease in bubble speed is observed for all reference bubble

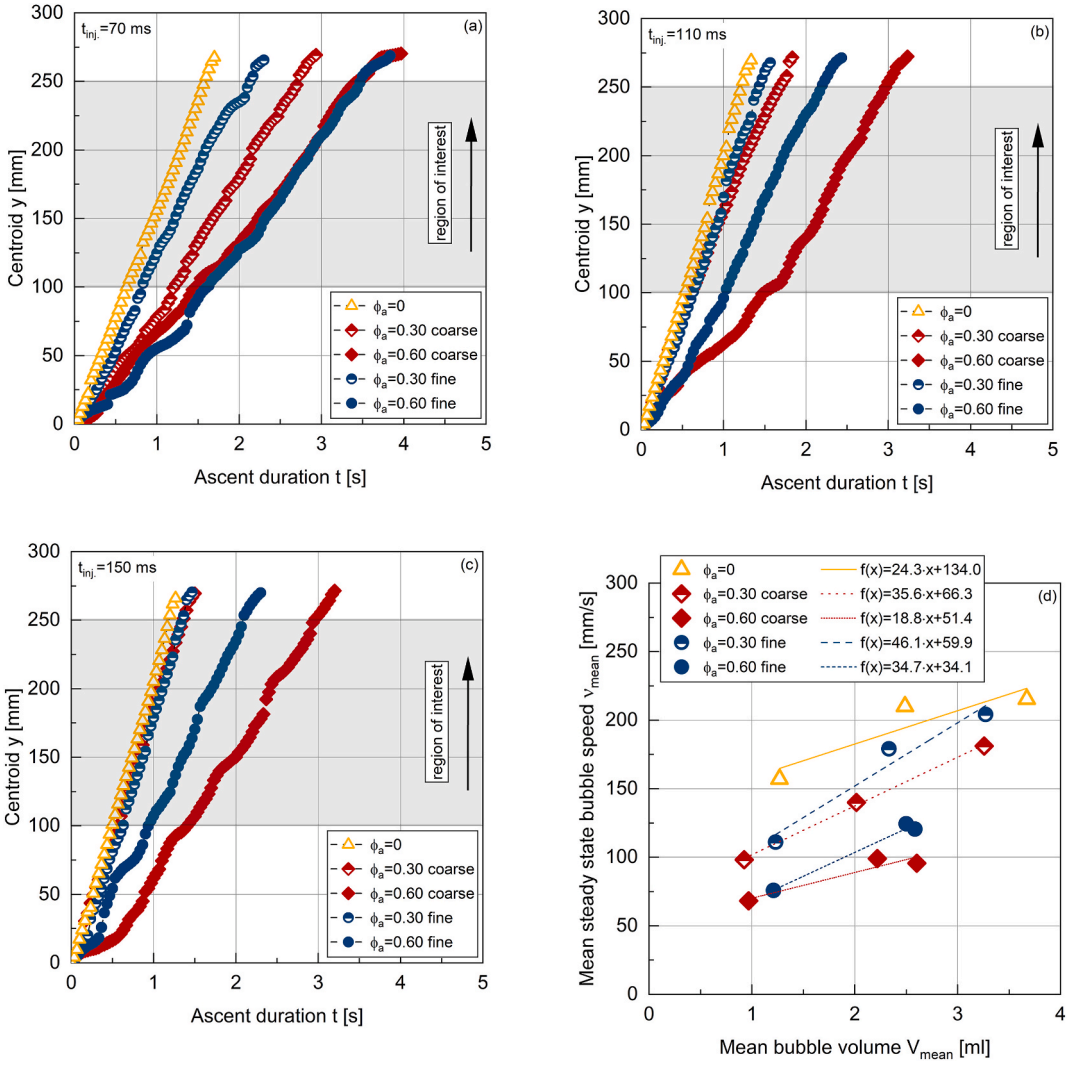

Fig. 4. Vertical bubble motion as a function of the ascent duration t for injection time $t_{inj.} = 70$ ms (a), $t_{inj.} = 110$ ms (b), $t_{inj.} = 150$ ms (c) and mean steady state bubble speed v_{mean} in the ROI as a function of the mean bubble volume V_{mean} (d); linear regressions functions shown in (d) used to compute the bubble speed of corresponding reference bubble volumes V_1 to V_3.

volumes, by addition of aggregates, which is consistent with the decreased flowability (cf. Table 5). For bubbles of volume $V_1 = 1$ ml, the reduction in bubble speed is almost linear for both 30 vol% and 60 vol% aggregates. However, there is a significant reduction from 157.3 mm/s for the pure paste to almost 100 mm/s for 30 vol% and almost 70 mm/s for 60 vol% aggregates, irrespective of whether fine or coarse-graded aggregates are used. By increasing the bubble volume to $V_2 = 2$ ml and thus the overall bubble speed, the effect of aggregate content and grading becomes more apparent. In this case, the reduction in bubble speed is more pronounced for the coarse particle size fractions. The bubble speed decreases from 181.6 mm/s for the pure paste to 152.0 mm/s for the fine and 137.5 mm/s for the coarse grading for 30 vol% aggregates. For 60 vol% aggregates, however, the bubble speed decreases to 103.5 mm/s for the fine and 88.92 mm/s for the coarse aggregates. The trend continues for the $V_3 = 3$ ml bubble volume and shows the most pronounced effects of grading, but the effect of 30 vol% aggregates is almost negligible for the fine-graded concrete as the bubble velocity only decreases from 205.9 mm/s to 198.1 mm/s. Presumably, the bubble is large enough and has sufficient buoyancy to push the smaller particles away without being decelerated or stopped. By using coarser aggregates, the bubble is slowed down more, resulting in a greater reduction in the mean bubble speed. The same phenomenon occurs with 60 vol% aggregate, but here the bubble also slows down with the finer aggregate, and the effect is much stronger with the coarser aggregates.

The effect of particle migration (i.e. particles pushed out of the way) during air bubble rise in cement paste was already been investigated by the authors in Refs. [3,12], where we pointed out that rising air bubbles create shear channels with less concentrated regions in the centre and increased particle packing at the channel walls. Therefore, another point of interest of this paper at hand was, if the same effect will occur when coarser aggregates are introduced. After the first bubble was injected into the sample, three subsequent bubbles were injected in a row with a 60 s s rest period between each bubble. Fig. 5(b)–(d) shows the steady state bubble speed

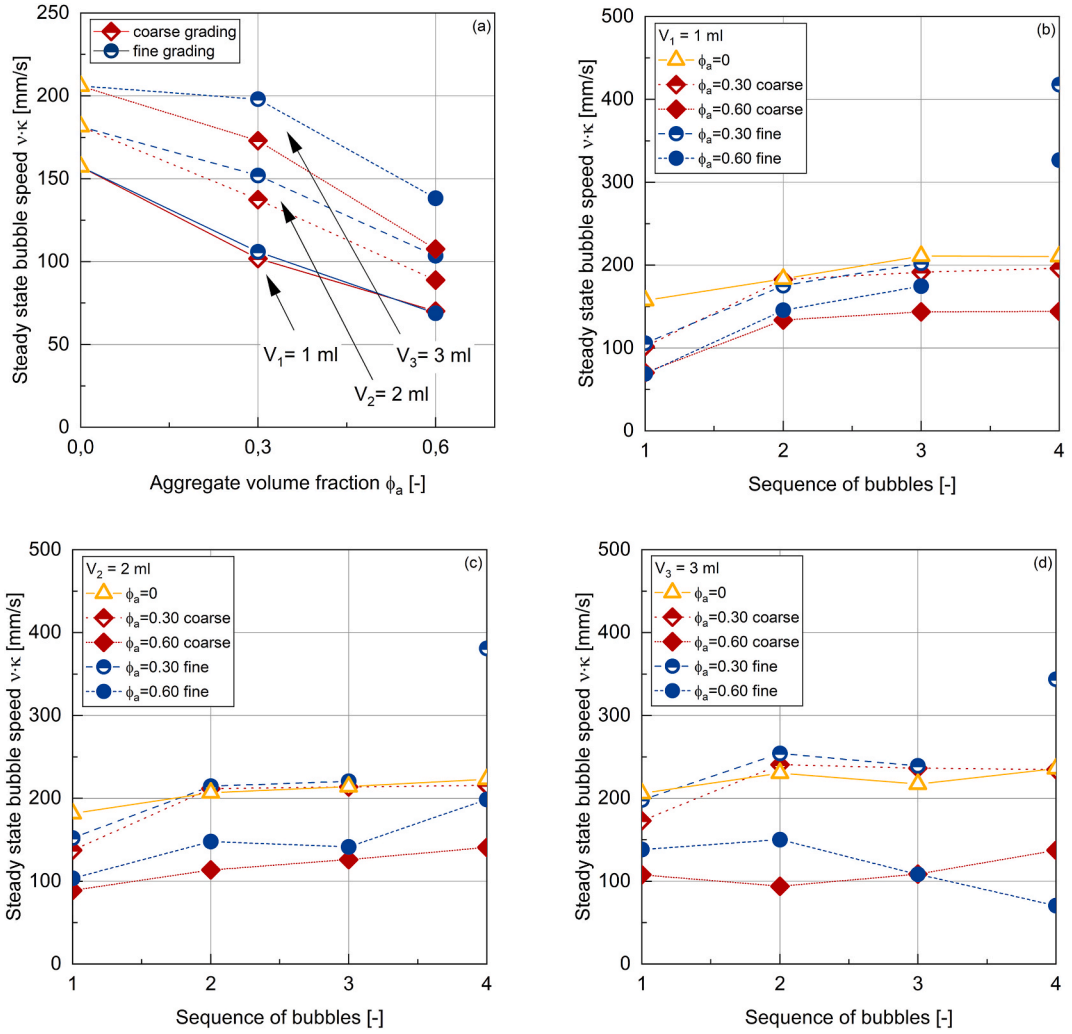

Fig. 5. Bubble size corrected steady state bubble speed v as a function of the aggregate volume fraction ϕ_a (a), as a function of the sequence of bubbles for bubble volumes of $V_1 = 1$ ml (b), $V_2 = 2$ ml (c) and $V_3 = 3$ ml (d).

Table 5
Spread flow and fresh concrete temperature of the investigated concretes.

ϕ_p_ϕ_a_grading	0.38_0_0	0.38_0.3_coarse	0.38_0.6_coarse	0.38_0.3_fine	0.38_0.6_fine
Spread flow [mm]	260	257.5	210	260	207.5
Temperature [°C]	22.2	20.2	20.4	22.1	22.5

of these 4 bubbles as a function of the sequence of bubbles for the bubble volumes of 1 ml, 2 ml and 3 ml.

Starting from the smallest bubble volume of 1 ml, it can be seen that the influence of fine or coarse grading becomes visible in the subsequent bubbles (cf. Fig. 5 (b)), which was not the case for the first bubbles in Fig. 5 (a). For the coarse-graded concretes, both the 30 vol% and 60 vol% concretes show an increased bubble speed for the second bubble compared to the first bubble, but the speed remains almost constant for the third and fourth bubbles. Compared to the fine-graded concrete, this concrete shows an increase in bubble speed with each subsequent bubble. It should be noted that the fourth bubble has to be considered as an outlier. The reason was found in unexplained changes in the image acquisition frame rate due to complications in the X-ray laboratory. These not assignable changes in frame rate result in increased bubble speeds, and have to be considered as artefacts.

By increasing the bubble volume to 2 ml and 3 ml (cf. Fig. 5(c)–(d)), it was found that the effect of the subsequent bubbles in the 60 vol% concretes become minor for both aggregate contents, i.e. the bubble velocity increases very little for 2 ml and remains almost constant for 3 ml bubble volume.

A rising bubble is capable of displacing aggregates and creating rise channels. However, fine aggregates are more readily displaced

than coarse aggregates, resulting in a greater increase in bubble velocity for subsequent bubbles. As the volume of the bubble increases, it would be expected that larger bubbles would more easily create rising channels and result in an increased bubble velocity. However, this was not observed. As the influence of aggregate content, rather than its 30 vol% or 60 vol%, becomes more significant in the ascent of larger subsequent bubbles, it can be proposed that larger bubbles may encounter greater difficulty in identifying and following the predefined path, potentially resulting in trajectory variations. These results will be further discussed in the subsequent section 3.4.

3.3. Trajectory

In addition to the bubble speed, we also measured the uprising path of the air bubbles. Fig. 6 shows the results of the trajectories along the *y*- and *x*-axis for all bubble sizes and mixture compositions investigated.

At the lower aggregate content of 30 vol%, all bubbles, small to large in volume, are able to rise almost vertically, with subsequent bubbles following the path of the previous one. By increasing the aggregate content to 60 vol%, the bubble starts to interact with the surrounding aggregates, and the interaction depends on the ratio of bubble size to aggregate size.

For all small bubbles (i.e. $t_{inj.} = 70$ ms), regardless of the solid volume fraction or aggregate grading, all subsequent bubbles follow the paths created by the first bubbles (i.e. the solid line). If we compare these findings with the data in Fig. 5 (b), we see that the corresponding bubble speed increases for each subsequent bubble.

For larger bubble volumes $t_{inj.} = 110$ ms and $t_{inj.} = 150$ ms, we found the same phenomena for the 30 vol% concretes measured for

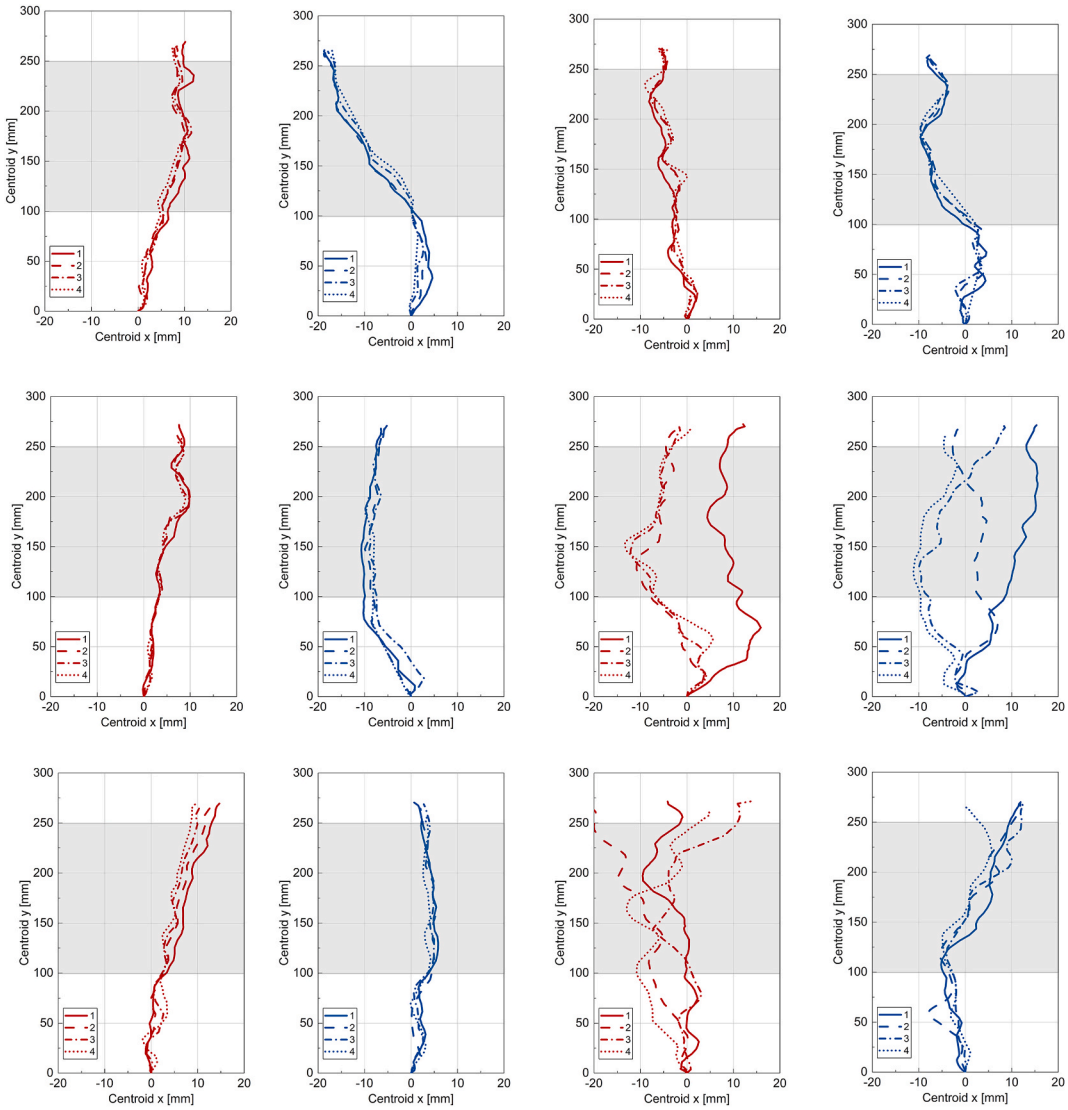

Fig. 6. Trajectory of the 4 injected air bubbles for all injection duration ($t_{inj.} = 70$ ms, 110 ms and 150 ms) and all mixture compositions. Note that the scale is not the same in x and y, exagerating the bubble trajectory deviation with respect to the vertical.

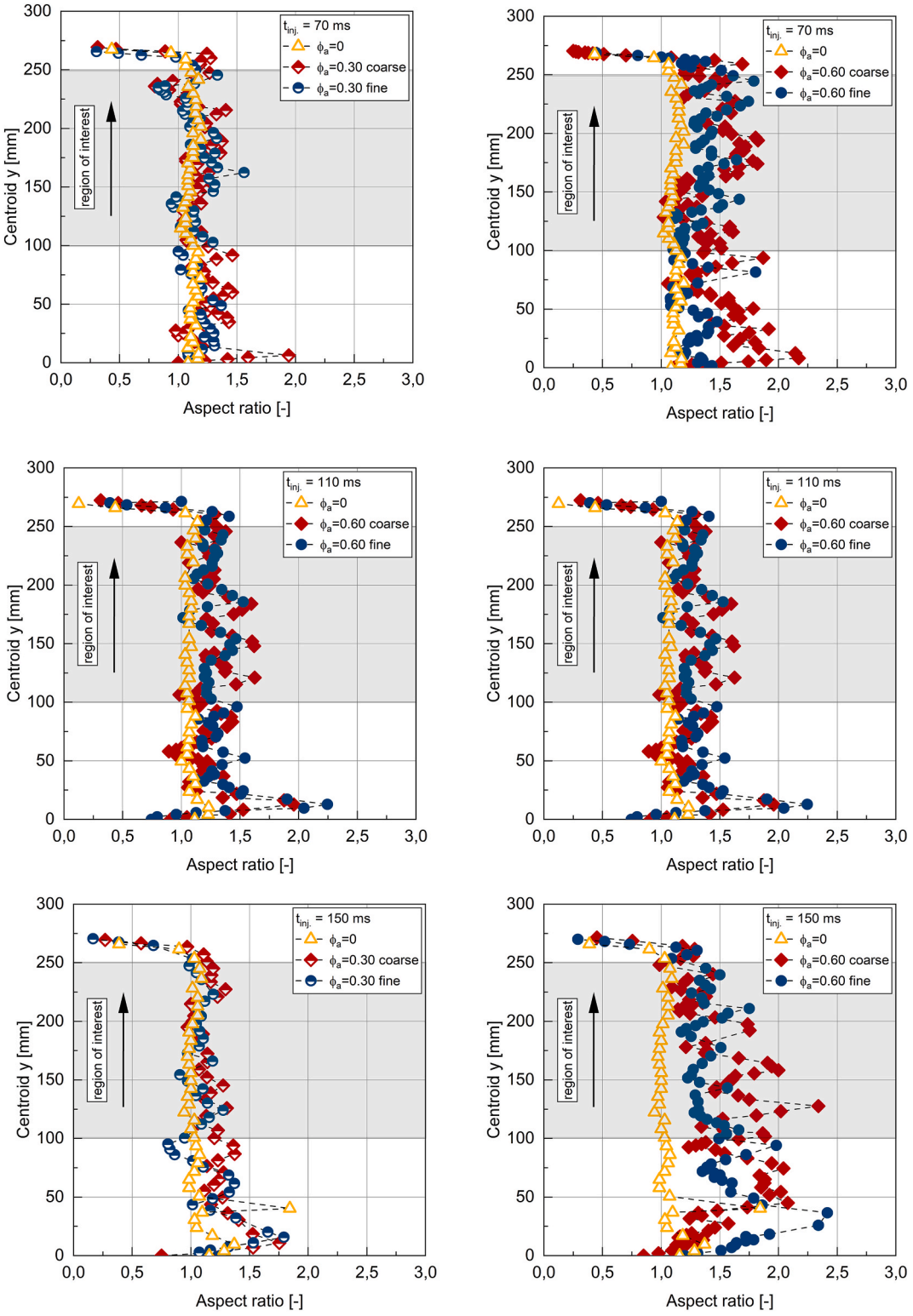

Fig. 7. Changes in bubble aspect ratio χ during vertical rise for the injection durations of $t_{inj.} = 70$ ms (top), $t_{inj.} = 110$ ms (middle) and $t_{inj.} = 150$ ms (bottom) with $\phi_a = 0.30$ (left) and $\phi_a = 0.60$ (right).

small bubbles, as all of the trajectories of the subsequent bubbles are almost the same and follow the first bubble. Furthermore, the trajectories are less far from vertical, which means that the larger bubble volumes are less affected by the small amount of aggregates compared to the shifted and wavy trajectories of the smaller bubbles. Aggregate grading shows no effect on trajectory in all mixes with only 30 vol% aggregates. Except for the test of the medium size bubble $t_{inj.} = 110$ ms in 60 vol% coarse aggregate, where only the first bubble has a different trajectory and the three subsequent bubbles have the same. All other mixtures having 60 vol% aggregate show a different behavior after the increase of aggregate volume fraction from 30 vol% to 60 vol%. We found different trajectories for every bubble, meaning each bubble creates its own new rising path and does not follow previously created rising channels.

By increasing the aggregate volume fraction to 60 vol% the aggregates suspension is so dense that it is dominated by interactions between particles and friction, and acts as a network of fixed obstacles. Due to their low buoyancy, the small bubbles can hardly move these obstacles, which may block the rise path for subsequent bubbles. The aggregates are very densely packed with such a packing density of 0.60 and are very close to the maximum packing density of approximately 0.64 for a random packing of monodispersed spherical beads [27].

For the individual case of the largest bubble and 60 vol% fine aggregates, we also found different trajectories, but the difference between them is less pronounced. This may be because the smaller aggregates have less inertia and are more easily moved out of the way of such large bubbles than the coarser aggregates, which have a larger inertia. Another hypothesis could be that channel walls made of smaller aggregates are less stable and can be broken more easily by a bubble than channels made of coarser aggregates.

3.4. Bubble aspect ratio

Fig. 7 shows the changes in bubble aspect ratio χ (i.e. bubble *y* elongation divided by bubble *x* elongation) for 30 vol% (left) and 60

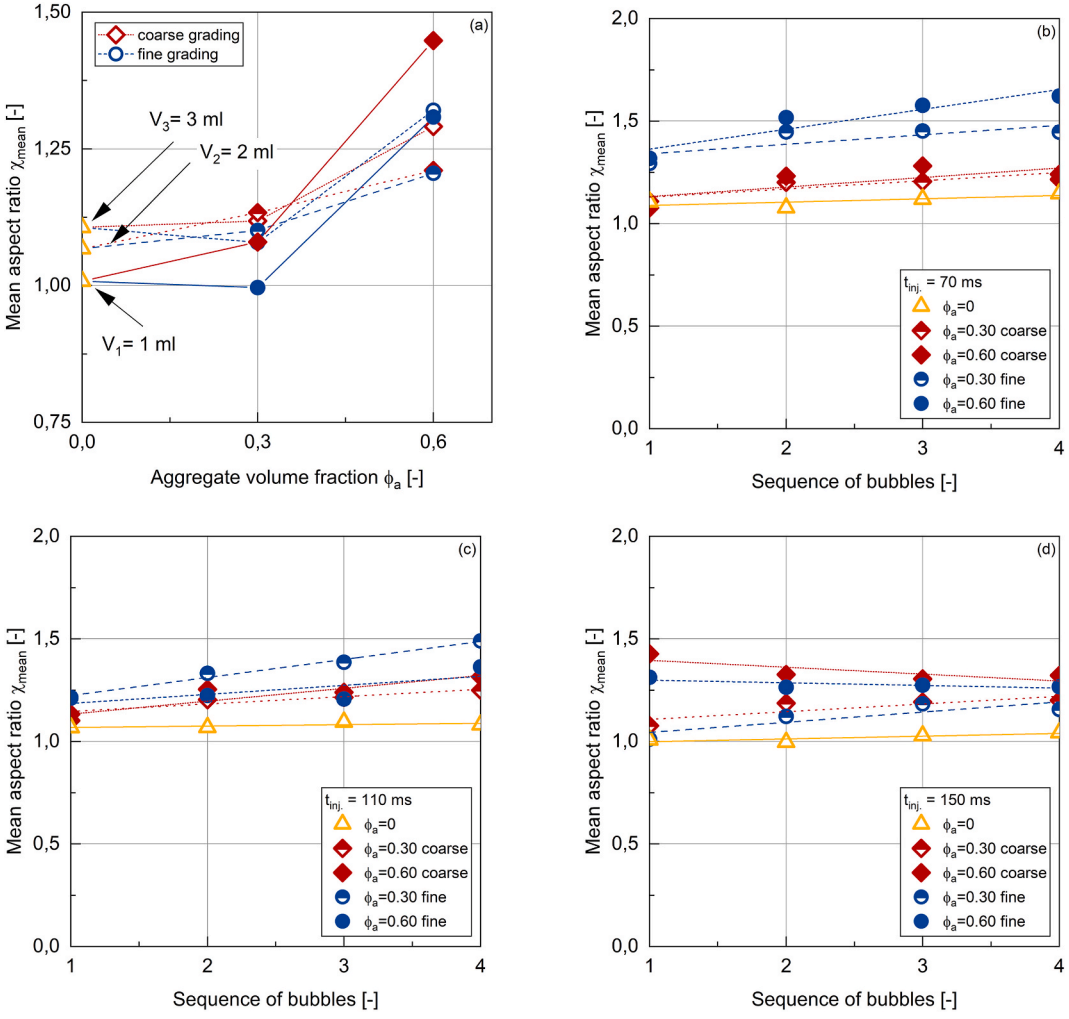

Fig. 8. Mean aspect ratio χ_{mean} as a function of the aggregate volume fraction ϕ_a for all concretes investigated (a) and as a function of the sequence of bubbles for the bubble volume $V_1 = 1$ ml (b); $V_2 = 2$ ml (c); $V_3 = 3$ ml (d).

vol% aggregate content (right) during vertical motion. The data points χ are computed framewise at a framerate of 30 fps.

Starting with pure cement paste, χ remains almost constant during the entire rise process. This behavior occurs for all bubble sizes, with χ increasing as the bubble size increases. By adding 30 vol% aggregates, χ only increases very little (i.e. the bubble becomes longer and narrower) but more importantly, χ starts to scatter along the rise pathway due to bubble-aggregate interactions. The effect of aggregate grading, whether coarse or fine, as well as varying bubble sizes, is not clear. Through the increase in the amount of aggregates from 30 vol% to 60 vol%, the general values of χ, and the scattering of the values increase very strong. Any change in a data point can be interpreted as a deformation of the bubble shape due to its interaction with the surrounding aggregates. Between the small bubble size with $t_{inj.} = 70$ ms and medium with $t_{inj.} = 110$ ms the differences in χ are apparently negligible. However, for the largest bubble size with $t_{inj.} = 150$ ms, the framewise changes in aspect ratio, and hence the bubble-aggregate interactions are evident in a pronounced scatter. Moreover, the effect of aggregate grading also plays a role for larger bubbles, as the coarse-graded concretes yield more pronounced bubble deformation than the fine-grained concretes.

For a more general comparison of the results, the mean values of the aspect ratio χ_{mean} over the region of interest are plotted as a function of the aggregate volume fraction ϕ_a in Fig. 8 (a). The first point of interest is that all values of χ_{mean} are larger than one, meaning the bubbles are more elliptical and elongated in the vertical direction (i.e $\chi_{mean} > 1$) than spherical or flat (i.e. $\chi_{mean} \leq 1$). As described qualitatively above, χ_{mean} of the rising air bubbles remains almost constant after increasing the aggregate content from 0 vol % to 30 vol%. Especially, the value of the small bubble volume in combination with the fine-graded concrete is completely unaffected by the aggregates and remains completely constant. Increasing ϕ_a to 60 vol%, results in significantly larger χ_{mean} values. The largest growth is observed for the largest bubble volume, as such large bubbles are less stable and are more easily deformed. Overall, it can be said that increased bubble volume, increased aggregate volume fraction, and the use of coarse-grading aggregates enhance bubble deformation and elongates the bubble in the vertical direction (i.e. increased χ_{mean}) the most.

The effect of the shear history on bubble deformations was investigated by plotting χ_{mean} as a function of the sequence of bubbles (see Fig. 8(b)–(d)). All subsequent bubbles show an increase in χ_{mean}, but differences can be seen when comparing the effect of aggregate grading. Hereby, Fig. 8 (b) shows the results for the small bubble volume ($t_{inj.} = 70$ ms). In pure cement paste, a growth in χ_{mean} is observed, however it is very small. Right above are the results for the coarse-graded concretes with both 30 vol% and 60 vol% of aggregates having almost the same values. The highest values were measured for the both fine-graded concretes, with slightly higher values for the 60 vol% aggregates. This order of the graphs remains the same for the medium bubble volume with $t_{inj.} = 110$ ms, but the linear regressions appear to be parallel shifted together so that the effect of the fine-grained concretes becomes less pronounced. Lastly, for the largest bubble ($t_{inj.} = 150$ ms), the linear regressions even become almost horizontal and the bubble deformations approach the behavior of a pure cement paste.

4. Shear-induced particle migration during bubble rise

One of the key findings of the study described in Refs. [3,12] and the paper at hand was that shear induced by a rising air bubble can lead to shear-induced particle migration with the development of shear channels in the fresh concrete. These channels have an increased water content in the centre (i.e. locally decreased viscosity) and an increased particle concentration at the channel walls, so that subsequent bubbles tend to follow these rise paths and have an increased rise speed.

The behavior of how particles in a suspension will react in a flow caused by the shear of a moving object (e.g. solid spheres or air bubbles), whether they will follow a change in flow or maintain their motion due to their inertia, can be described by the Stokes number *St*. This dimensionless number indicates the ratio of the inertial forces of the particles (i.e. the response time of the particle t_p) to the characteristic time of the air bubble t_b and can be computed with equation Eq. (1) [28,29].

$$St = \frac{t_p}{t_b} \quad \text{Eq. 1}$$

The response time t_p of the particles is a function of the particle density ρ_p, the particle diameter d_s and the viscosity of the surrounding cement paste $\eta(\dot{\gamma})$. The characteristic time of the air bubble t_b is computed by the ratio of the bubble diameter d_b and the bubble speed in steady state v_b.

$$t_p = \frac{\rho_p \cdot {d_s}^2}{18 \cdot \eta(\dot{\gamma})} \quad \text{Eq. 2}$$

$$t_b = \frac{d_b}{v_b} \quad \text{Eq. 3}$$

We first calculated the Stokes numbers of the individual aggregates in the polydisperse distribution of particle sizes and found an increase in Stokes number with increasing aggregate diameter. For instance, a reference bubble volume $V_1 = 1$ ml in the 30 vol% coarse-graded concrete, results in individual values of Stokes number $St_{ind.} = 2.99$ (for $d_a = 2$ mm); $St_{ind.} = 11.98$ (for $d_a = 4$ mm) and $St_{ind.} = 47.27$ (for $d_a = 8$ mm). The increase in Stokes number is in line with the expectation that larger particles are more resistant to shear-induced particle migration due to their increased inertia. We calculate the total Stokes number $St_{tot.}$ Corresponding to the polydisperse distribution by weighting the individual Stokes numbers by their corresponding volumetric contents in the particle size distribution. This gives, for instance a total Stokes number for the smallest bubble sizes in the coarse-graded concrete of $St_{tot.\ coarse} = 22.00$ and $St_{tot.\ fine} = 16.59$ for the fine-graded concrete. The comparison of these two values suggests that the aggregates in the fine-

graded concrete are less stable against particle migration than those in the coarse-graded concrete with higher Stokes numbers. This confirms the above-described findings in the experimental results, that coarse aggregates reduce the bubble speed more than fine aggregates and that they lead to stonger bubble deformations. According to the literature, the magnitude of the observed Stokes numbers can be interpreted as the capability of a given bubble to migrate aggregates of all three diameters [29], but the intensity of aggregate migration decreases with aggregate size and hence Stokes number. It should be noted, however, that the interpretation of Stokes numbers is only valid for individual particles affected by the flow, which is why we have only used the results for concretes with 30 vol% aggregates, where we assume that the aggregates are not densely packed, in this interpretation. Densely packed aggregates, i. e. 60 vol%, where the aggregates mechanically interact with each other, cannot be considered because the packing density is not included in the Stokes consideration (i.e. Eq. (1) - Eq. (3)).

5. Conclusions

This paper presents an experimental study of how individual air bubbles rise in fresh concrete with different granulometric properties. The de-airing tests were carried out using X-ray imaging techniques to detect dynamic air bubble parameters during their movement. In addition to different bubble volumes, the effect of three volumetric aggregate contents (0 vol%, 30 vol% and 60 vol%) and the effect of aggregate grading (fine and coarse) on bubble speed, trajectory and bubble deformation (i.e. changes in aspect ratio) were investigated. The effect of shear-induced particle migration concerning shear history was also of interest.

In general, we found that the de-airing of fresh concrete is significantly influenced by the addition of aggregates. Especially for aggregate contents of 60 vol% close to the maximum packing density, the bubble rise is no longer continuous, but rather experiences a stop and go dynamics due to the bubble-aggregate interactions.

The bubble speed decreases with reduced bubble volume and increased aggregate content from 0 vol% to 30 vol% and 60 vol%. For large bubbles, coarse-graded concrete slows bubble speed more than fine-graded concrete, but this effect diminishes with medium bubbles and is negligible for small bubbles. Larger bubbles move particles more easily, while smaller bubbles are not able to move either of these aggregates, so particle size plays a minor role here.

The effect of the shear history was investigated by injecting three subsequent bubbles after the primary bubble. The greatest increase in bubble speed was observed between the first and second bubbles, with the subsequent bubbles showing slower speeds. As the bubble volume increases, this phenomenon becomes less intense and the differences between 30 vol% and 60 vol% aggregate content become more visible, i.e. the bubble speed pronounced very little or remains almost constant for the largest bubble volumes and 60 vol %. Overall, the coarse graded concretes show a slower bubble velocity than the fine graded concretes.

In parallel with the bubble speed, we have shown the effect of shear history on the bubble rise trajectories. For small volumes, trajectories in 30 vol% and 60 vol% aggregates, across both gradings, appear similar with slight zigzag and wavy paths, as small bubbles “squeeze”through the aggregate network. For larger bubble volumes, this phenomenon is still true for 30 vol% of aggregates, regardless of the aggregate grading used. However, at 60 vol%, the trajectories vary for successive bubbles due to aggregates approaching maximum packing density, so that the aggregates support themselves and do not create a rise channel. This behavior is confirmed by the corresponding bubble speeds, which also remain almost constant and do not increase with each subsequent bubble.

The final parameter investigated was bubble deformation due to bubble-aggregate interactions. It was found that 30 vol% of aggregates do not affect the bubble shape for all bubble volumes. It is only when the aggregate content is increased to 60 vol% that a change in the bubble aspect ratio is observed, but this becomes more pronounced as the bubble volume increases. Finally, concrete grading also has an effect, as the largest bubble deformations occur with large bubble volumes and 60 vol% coarse aggregates. The shear history shows its strongest effect for the smallest bubbles, as subsequent bubbles have strongly increased mean aspect ratio χ_{mean}. When the bubble volume increases χ_{mean} becomes less influenced by the sequence of bubbles. In addition, we have shown that the use fine aggregates results in a higher χ_{mean} compared to coarse aggregates.

These results are consistent with the above-mentioned results and confirm that shear-induced particle migration occurs during bubble rise, depending on the bubble volume and the granulometry of the aggregates. The dimensionless Stokes number St was used to determine the tendency of the aggregates to move due to flow. However, St only works for single objects, i.e. single aggregates, and not for networks of interacting particles as the packing density is not included in the equation (cf. Eq. (2) and Eq. (3)). Even if we assume that for concretes with low aggregate contents that the aggregates are well dispersed in the cement paste with sufficient spacing between them, the use of St to determine the behavior of concrete aggregates must be considered with caution. This paper result fits well with the result of the previous paper [3] where we showed the limits of the use of the dimensionless Reynolds number Re to determine bubble rise in cement paste. The physical fundamentals of bubble rise in fluids and granular suspensions cannot be fully used to describe bubble rise in cement paste or concrete. Here we are dealing with highly thixotropic granular suspensions with a very wide particle size and size distribution and a tendency to segregate during shear-induced particle migration. However, such work is taking a decisive step in the closing of this research gap.

CRediT authorship contribution statement

Bastian Strybny: Writing – original draft, Visualization, Methodology, Investigation, Data curation, Conceptualization. **Max Coenen:** Writing – review & editing, Visualization, Software. **Valérie Vidal:** Writing – review & editing, Supervision, Methodology. **Tobias Schack:** Writing – review & editing, Methodology. **Marcus Zuber:** Software, Investigation. **Michael Haist:** Writing – review & editing, Supervision, Methodology, Funding acquisition.

Declaration of competing interest

The authors declare the following financial interests/personal relationships which may be considered as potential competing interests: Prof. Dr.-Ing. Michael Haist reports financial support was provided by Deutsche Forschungsgemeinschaft (DFG). If there are other authors, they declare that they have no known competing financial interests or personal relationships that could have appeared to influence the work reported in this paper.

Acknowledgements

This research was funded by Deutsche Forschungsgemeinschaft (DFG) under the grants HA 7917/8–1, LU 1652/48-1 SCHA 1854/7–1 and within the DFG priority program 2005 “Opus Fluidum Futurum—Rheology of reactive, multiscale, multiphase construction materials”.

Data availability

Data will be made available on request.

References

[1] N. Roussel, G. Ovarlez, S. Garrault, C. Brumaud, The origins of thixotropy of fresh cement pastes, Cement Concr. Res. 42 (1) (2012) 148–157, https://doi.org/10.1016/j.cemconres.2011.09.004.
[2] P. Banfill (Ed.), The Rheology of Fresh Cement and Concrete - a Review, 2003.
[3] B. Strybny, et al., Mechanisms of air bubble rise in cement suspensions studied by X-ray analysis, Constr. Build. Mater. 457 (2024) 139330, https://doi.org/10.1016/j.conbuildmat.2024.139330.
[4] W.B. Fuller, S.E. Thompson, The laws of proportioning concrete, Trans. Am. Soc. Civ. Eng. 59 (2) (1907) 67–143, https://doi.org/10.1061/TACEAT.0001979.
[5] A. H. M. Andreasen and J. Andersen, "Ueber die Beziehung zwischen Kornabstufung und Zwischenraum in Produkten aus losen Körnern (mit einigen Experimenten)," Colloid Polym. Sci., Vol. 50 (3), pp. 217–228.
[6] J.E. Funk, D.R. Dinger, Predictive Process Control of Crowded Particulate Suspensions: Applied to Ceramic Manufacturing, s.l.: Springer US, Boston, MA, 1994.
[7] F.d. Larrard, Concrete Mixture Proportioning: a Scientific Approach, CRC Press, 1999.
[8] S.A.A.M. Fennis, Design of Ecological Concrete by Particle Packing Optimization," Dissertation, Technische Universiteit Delft, Delft, 2011 [Online]. Available: http://repository.tudelft.nl/view/ir/uuid:5a1e445b-36a7-4f27-a89a-d48372d2a45c.
[9] A.K.H. Kwan, C.F. Mora, Effects of Various Shape Parameters on Packing of Aggregate Particles, 2001.
[10] B.M. Aïssoun, S.-D. Hwang, K.H. Khayat, Influence of aggregate characteristics on workability of superworkable concrete, Mater. Struct. 49 (1–2) (2016) 597–609, https://doi.org/10.1617/s11527-015-0522-9.
[11] S.A. Fennis, J.C. Walraven, Using particle packing technology for sustainable concrete mix design, Heron 57 (2) (2012) 73–102.
[12] B. Strybny, J. Link, M. Coenen, M. Zuber, Tobias Schack, M. Haist (Eds.), De-airing of Fresh Concrete - Unraveling the Mechanisms of a Very Old Problem: Proc. of the 15th Fib International Phd Symposium in Civil Engineering, 2024.
[13] S. Fataei, "Flow-Induced Particle Migration in Concrete Under High Shear Rates," Dissertation, Technische Universität Dresden.
[14] G.K. Auernhammer, et al., Transparent model concrete with tunable rheology for investigating flow and particle-migration during transport in pipes, Mater. Des. 193 (2020) 108673, https://doi.org/10.1016/j.matdes.2020.108673.
[15] M.N. Kluwe, M.A. Haustein, R. Schwarze, Optical investigation of dense suspensions with Non-Newtonian matrix under pulsating pumping, J. Non-Newtonian Fluid Mech. 303 (2022) 104778, https://doi.org/10.1016/j.jnnfm.2022.104778.
[16] U. Pott, et al., Characterization data of reference materials used for phase II of the priority program DFG SPP 2005 "opus fluidum futurum - rheology of reactive, multiscale, multiphase construction materials, Data Brief 47 (2023) 108902, https://doi.org/10.1016/j.dib.2023.108902.
[17] DIN EN 1097-7:2008-06, Tests for Mechanical and Physical Properties of Aggregates - Part 7: Determination of the Particle Density of Filler - Pyknometer Method; German version *EN 1097-7*:2008, Berlin.
[18] DIN ISO 9277:2014-01, Determination of the Specific Surface Area of Solids by Gas Adsorption - BET Method (ISO 9277:2010), Berlin.
[19] DIN EN 196-6:2019-03, Methods of Testing Cement - Part 6: Determination of Fineness; German version EN 196-6:2018, Berlin.
[20] DIN ISO 13320:2022-12, Partikelgrößenanalyse_- Laserbeugungsverfahren (ISO_13320, 2020. Berlin.
[21] DIN EN 196-2, Prüfverfahren Für Zement_- Teil_2: Chemische Analyse Von Zement; Deutsche Fassung EN_196-2:2013, 2013-10. Berlin.
[22] DIN 1045-2:2023-08, Tragwerke aus Beton, Stahlbeton Und Spannbeton_- Teil_2: Beton, Berlin.
[23] Methods of Test for Mortar Masonry - Part 3: Determination of Consistency of Fresh Mortar (by flow table): Beuth, Berlin, Berlin.
[24] M. Haist, et al., Interlaboratory study on rheological properties of cement pastes and reference substances: comparability of measurements performed with different rheometers and measurement geometries, Mater. Struct. 53 (4) (2020), https://doi.org/10.1617/s11527-020-01477-w.
[25] M. Haist, Zur Rheologie und den Wechselwirkungen bei Zementsuspensionen, in: Dissertation, Institut Für Massivbau Und Baustofftechnologie (IMB), 2009. Universität Karlsruhe (TH), Karlsruhe.
[26] M. Zuber, Development, characterization and application of a novel X-ray imaging laboratory. Institute for Photon Science and Synchrotron Radiation, Karlsruhe Institute of Technology, Karlsruhe, 2023. Dissertation.
[27] G.D. Scott, D.M. Kilgour, The density of random close packing of spheres, J. Phys. D Appl. Phys. 2 (6) (1969) 863–866, https://doi.org/10.1088/0022-3727/2/6/311.
[28] Y. Tagawa, J.M. Mercado, V.N. Prakash, E. Calzavarini, C. Sun, D. Lohse, Three-dimensional lagrangian voronoï analysis for clustering of particles and bubbles in turbulence, J. Fluid Mech. 693 (2012) 201–215, https://doi.org/10.1017/jfm.2011.510.
[29] N. Hooshyar, J.R. van Ommen, P.J. Hamersma, S. Sundaresan, R.F. Mudde, Dynamics of single rising bubbles in neutrally buoyant liquid-solid suspensions, Phys. Rev. Lett. 110 (24) (2013) 244501, https://doi.org/10.1103/PhysRevLett.110.244501.